

# 1 Favipiravir and severe acute respiratory syndrome coronavirus 2 in hamster 2 model

3 Jean-Sélim Driouich<sup>1#</sup>, Maxime Cochin<sup>1#</sup>, Guillaume Lingas<sup>2</sup>, Grégory Moureau<sup>1</sup>, Franck Touret<sup>1</sup>, Paul  
4 Rémi Petit<sup>1</sup>, Géraldine Piorkowski<sup>1</sup>, Karine Barthélémy<sup>1</sup>, Bruno Coutard<sup>1</sup>, Jérémie Guedj<sup>2</sup>, Xavier de  
5 Lamballerie<sup>1</sup>, Caroline Solas<sup>1,3</sup>, Antoine Nougairède<sup>1\*</sup>

6 <sup>1</sup>: Unité des Virus Émergents, UVE: Aix Marseille Univ, IRD 190, INSERM 1207, Marseille, France.

7 <sup>2</sup>: Université de Paris, IAME, INSERM, F-75018 Paris, France

8 <sup>3</sup>: Laboratoire de Pharmacocinétique et Toxicologie, Hôpital La Timone, APHM, Marseille, France

9 #Contributed equally

10 \*Corresponding author: [antoine.nougairède@univ-amu.fr](mailto:antoine.nougairède@univ-amu.fr)

## 11 Summary

12 There is a need for safe and effective antiviral molecules with which to combat COVID-19 pandemics.  
13 Recently, *in vitro* inhibitory activity of favipiravir against SARS-CoV-2 was reported. Here, we used a  
14 Syrian hamster model to explore the pharmacokinetics of this molecule and its *in vivo* efficacy against  
15 SARS-CoV-2. Results revealed that high doses (700-1400mg/kg/day) significantly reduced virus  
16 replication in the lungs accompanied by clinical alleviation of the disease. However, these high doses  
17 were associated with significant toxicity in hamsters. Favipiravir pharmacokinetics displayed non-linear  
18 increase in plasma exposure between the doses and good lung penetration. Analysis of viral genomes  
19 *in vivo* showed that favipiravir induced a mutagenic effect. Whilst the plasma trough concentrations  
20 observed in this study were comparable with those previously found during human clinical trials, this  
21 potential toxicity requires further investigation to assess whether a tolerable dosing regimen can be  
22 found in humans that effectively reduces virus replication.

## 23 Keywords

24 COVID-19, SARS-CoV-2, antiviral therapy, favipiravir, animal model, preclinical research

## 25 Introduction

26 In March 2020, the World Health Organization declared coronavirus disease 2019 (COVID-19) a  
27 pandemic (WHO, 2020). The COVID-19 outbreak was originally identified in Wuhan, China, in  
28 December 2019 and spread rapidly around the world within a few months. The severe acute  
29 respiratory syndrome coronavirus 2 (SARS-CoV-2), the causative agent of COVID-19, belongs to the  
30 *Coronaviridae* family and is closely related to the SARS-CoV which emerged in China in 2002 (Zhu et  
31 al., 2020). After an incubation period of about 5 days, disease onset usually begins with an influenza-  
32 like syndrome associated with high virus replication in respiratory tracts (Huang et al., 2020, He et al.,  
33 2020). In some patients, a late acute respiratory distress syndrome, associated with high levels of  
34 inflammatory proteins, occurs within one to two weeks (Huang et al., 2020). As of 7 July 2020, more  
35 than 11.6 million cases of COVID-19 have resulted in more than 538,000 deaths (Dong et al., 2020). In  
36 the face of this ongoing pandemic and its unprecedented repercussions, not only on human health but  
37 also on society, ecology and economy, there is an urgent need for effective infection prevention and  
38 control measures.

39 Whilst host-directed and immune-based therapies could prove useful for the clinical management of  
40 critically ill patients, the availability of safe and effective antiviral molecules would represent an  
41 important step towards fighting the current pandemic. As conventional drug development is a slow  
42 process, repurposing of drugs already approved for any indication was extensively explored and led to  
43 the implementation of many clinical trials for the treatment of COVID-19 (Mercorelli et al., 2018).  
44 However, the development of effective antiviral drugs for the treatment of COVID-19, should, as much  
45 as possible, rely on robust pre-clinical *in vivo* data, not only on efficacy generated *in vitro*. Accordingly,  
46 rapid implementation of rodent and non-human primate animal models should help to assess more  
47 finely the potential safety and efficacy of drug candidates and to determine appropriated dose  
48 regimens in humans (Chan et al., 2020, Rockx et al., 2020).

49 Favipiravir (6-fluoro-3-hydroxypyrazine-2-carboxamine) is an anti-influenza drug approved in Japan  
50 that has shown broad-spectrum antiviral activity against a variety of other RNA viruses (Guedj et al.,  
51 2018, Yamada et al., 2019, Segura Guerrero et al., 2018, Tani et al., 2018, Jochmans et al., 2016,  
52 Takahashi et al., 2003, Rosenke et al., 2018). Favipiravir is a prodrug that is metabolized intracellularly  
53 into its active ribonucleoside 5'-triphosphate form that acts as a nucleotide analogue to selectively  
54 inhibit RNA-dependent RNA polymerase and induce lethal mutagenesis (Baranovich et al., 2013,  
55 Sangawa et al., 2013). Recently, several studies reported *in vitro* inhibitory activity of favipiravir against  
56 SARS-CoV-2 with 50% effective concentrations (EC<sub>50</sub>) ranging from 62 to >500µM (10 to >78µg/mL)  
57 (Wang et al., 2020, Jeon et al., 2020, Shannon et al., 2020). Based on these results, more than 20 clinical  
58 trials on the management of COVID-19 by favipiravir are in progress (<https://clinicaltrials.gov/>). In the

59 present study, a Syrian hamster model (*Mesocricetus auratus*) was implemented to explore the *in vivo*  
60 safety and efficacy and the pharmacokinetics (PK) of several dosing regimens of favipiravir.

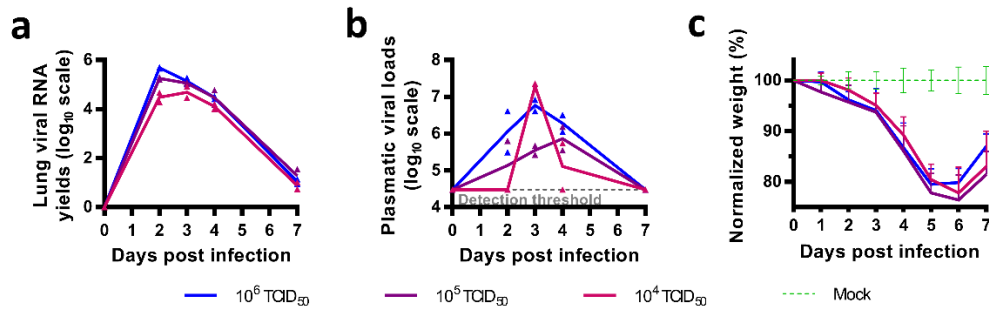
## 61 Results

### 62 *In vitro* efficacy of favipiravir

63 Using VeroE6 cells and an antiviral assay based on reduction of cytopathic effect (CPE), we recorded  
64  $EC_{50}$  and  $EC_{90}$  of 32 and 52.5  $\mu\text{g}/\text{mL}$  using a multiplicity of infection (MOI) of 0.001, 70.0 and  $>78.5\mu\text{g}/\text{mL}$   
65 with an MOI of 0.01 (Figure S1) in accordance with previous studies (Wang et al., 2020, Jeon et al.,  
66 2020, Shannon et al., 2020). Infectious titer reductions (fold change in comparison with untreated cells)  
67 were  $\geq 2$  with 19.6 $\mu\text{g}/\text{mL}$  of favipiravir and ranged between 11 and 342 with 78.5 $\mu\text{g}/\text{mL}$ . Using CaCo2  
68 cells, which do not exhibit CPE with SARS-CoV-2 BavPat1 strain, infectious titer reductions were around  
69 5 with 19.6 $\mu\text{g}/\text{mL}$  of favipiravir and ranged between 144 and 7721 with 78.5 $\mu\text{g}/\text{mL}$  of the drug. 50%  
70 cytotoxic concentrations ( $CC_{50}$ ) in VeroE6 and CaCo2 cells were  $>78.5\mu\text{g}/\text{mL}$ .

### 71 Infection of Syrian hamsters with SARS-CoV-2

72 Following Chan *et al.*, we implemented a hamster model to study the efficacy of antiviral compounds  
73 (Chan et al., 2020). Firstly, we intranasally infected four-week-old female Syrian hamsters with  $10^6$   
74  $TCID_{50}$  of virus. Groups of two animals were sacrificed 2, 3, 4 and 7 days post-infection (dpi). Viral  
75 replication was quantified in sacrificed animals by RT-qPCR in organs (lungs, brain, liver, small/large  
76 bowel, kidney, spleen and heart) and plasma. Viral loads in lungs peaked at 2 dpi, remained elevated  
77 until 4 dpi and dramatically decreased at 7 dpi (Figure 1a). Viral loads in plasma peaked at 3 dpi and  
78 viral replication was detected in the large bowel at 2 dpi (Figure 1b and Table S1). No viral RNA was  
79 detected in almost all the other samples tested (Table S1). Subsequently, we infected animals with two  
80 lower doses of virus ( $10^5$  and  $10^4$   $TCID_{50}$ ). Viral RNA was quantified in lungs, large bowel and plasma  
81 from sacrificed animals 2, 3, 4 and 7 dpi (Figure 1a and 1b). Viral loads in lungs peaked at 2 and 3 dpi  
82 with doses of  $10^5$  and  $10^4$   $TCID_{50}$  respectively. Maximum viral loads in lungs of animals infected with  
83 each dose of virus were comparable. Viral RNA yields in plasma and large bowel followed a similar  
84 trend but with more variability, with this two lower doses. In addition, clinical monitoring of animals  
85 showed no marked symptoms of infection but significant weight losses from 3 dpi when compared to  
86 animals intranasally inoculated with sodium chloride 0.9% (Figure 1c).



87

## 88 **Figure 1: Implementation of hamster model**

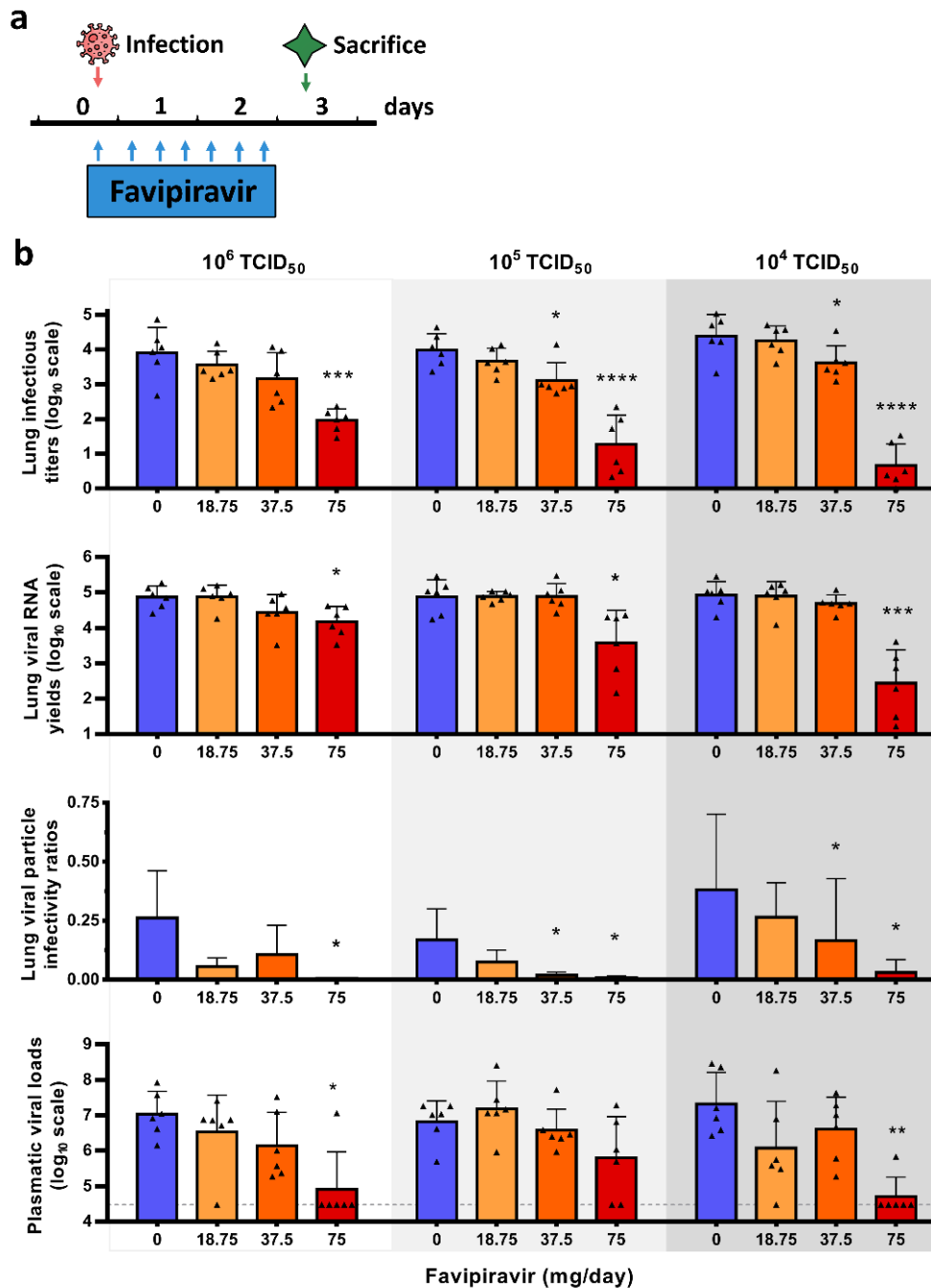
89 Hamsters were intranasally infected with 10<sup>6</sup>, 10<sup>5</sup> or 10<sup>4</sup> TCID<sub>50</sub> of virus. Viral replication was quantified using  
90 an RT-qPCR assay. **a** Lung viral RNA yields. **b** Plasmatic viral loads. **c** Clinical course of the disease. Normalized  
91 weight at day *n* was calculated as follows: (% of initial weight of the animal at day *n*)/(mean % of initial weight  
92 for mock-infected animals at day *n*). Data represent mean ±SD (details in Table S1).

## 93 *In vivo* efficacy of favipiravir

94 To assess the efficacy of favipiravir, hamsters received the drug, intraperitoneally, three times a day  
95 (TID). We used three doses of favipiravir: 18.75, 37.5 and 75mg/day (corresponding to 340±36, 670±42  
96 and 1390±126 mg/kg/day respectively).

97 In a first set of experiments, treatment was initiated at day of infection (preemptive antiviral therapy)  
98 and ended at 2 dpi. We infected groups of 6 animals intranasally with three doses of virus (10<sup>6</sup>, 10<sup>5</sup> and  
99 10<sup>4</sup> TCID<sub>50</sub>) and viral replication was measured in lungs and plasma at 3 dpi (Figure 2a). When analysis  
100 of virus replication in clarified lung homogenates was based on infectious titers (as measured using  
101 TCID<sub>50</sub> assay), an inverse relationship was observed between infectious titers and the dose of  
102 favipiravir (Figure 2b). This trend was even more important when low doses of virus were used to infect  
103 animals. At each dose of virus, mean infectious titers for groups of animals treated with 75mg/day TID  
104 were significantly lower than those observed with untreated groups ( $p \leq 0.0001$ ): reduction of infectious  
105 titers ranged between 1.9 and 3.7 log<sub>10</sub>. For animals infected with 10<sup>5</sup> or 10<sup>4</sup> TCID<sub>50</sub>, significant  
106 infectious titer reductions of around 0.8 log<sub>10</sub> were also observed with the dose of 37,5mg/day TID  
107 ( $p \leq 0.038$ ). Drug 90% and 99% effective doses (ED<sub>90</sub> and ED<sub>99</sub>) were estimated based on these results  
108 and ranged between 31-42mg/day and 53-70mg/day respectively (Table 2). When analysis of virus  
109 replication in clarified lung homogenates were assessed on viral RNA yields (as measured using  
110 quantitative real time RT-PCR assay), significant differences with groups of untreated animals, ranging  
111 between 0.7 and 2.5 log<sub>10</sub>, were observed only with the higher dose of favipiravir ( $p \leq 0.012$ ). Once  
112 again, this difference was more noticeable with lower doses of virus (Figure 2b). Since we found higher  
113 reductions of infectious titers than those observed with viral RNA yields, we estimated the relative  
114 infectivity of viral particle (*i.e.* the ratio of the number of infectious particles over the number of viral  
115 RNA molecules). Decreased infectivity was observed in all treated groups of animals. These differences

116 were always significant with the higher dose of favipiravir ( $p \leq 0.031$ ) and were significant with the dose  
 117 of 37.5mg/day TID for animals infected with  $10^5$  or  $10^4$  TCID<sub>50</sub> of virus ( $p \leq 0.041$ ). We then measured  
 118 plasmatic viral loads using quantitative real time RT-PCR assay and found, with the higher dose of  
 119 favipiravir and the groups of animals infected with  $10^6$  or  $10^4$  TCID<sub>50</sub>, significant reductions of 2.1 and  
 120 2.62 log<sub>10</sub>, respectively ( $p \leq 0.022$ ) (Figure 2b).



121

122 **Figure 2: Virological results with preemptive favipiravir therapy**

123 **a** Experimental timeline. **b** Viral replication in lungs and plasma. Hamsters were intranasally infected with  $10^6$ ,  
 124  $10^5$  or  $10^4$  TCID<sub>50</sub> of virus. Lung infectious titers (measured using a TCID<sub>50</sub> assay) and viral RNA yields were  
 125 (measured using an RT-qPCR assay) expressed in TCID<sub>50</sub>/copy of  $\gamma$ -actine gene and viral genome copies/copy of

126  $\gamma$ -actine gene respectively. Relative lung viral particle infectivities were calculated as follows: ratio of lung  
127 infectious titer over viral RNA yields. Plasmatic viral loads (measured using an RT-qPCR assay) are expressed in  
128 viral genome copies/mL of plasma (the dotted line indicates the detection threshold of the assay). Data represent  
129 mean  $\pm$ SD. \*\*\*\*, \*\*\*, \*\* and \* symbols indicate that the average value for the group is significantly lower than  
130 that of the untreated group with a p-value  $<0.0001$ , ranging between 0.0001-0.001, 0.001-0.01 and 0.01-0.05  
131 respectively (details in Table S2 and S3).

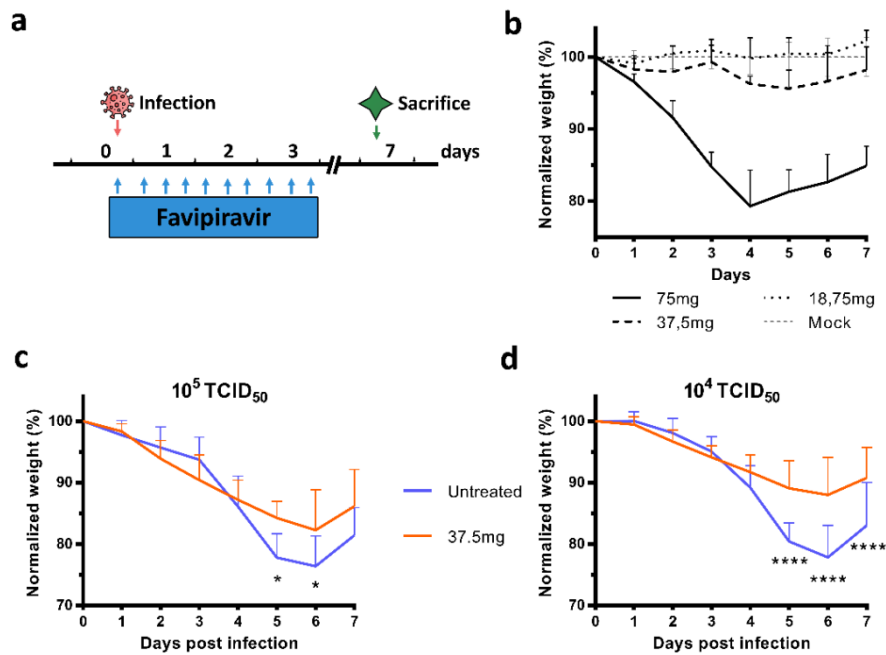
132 **Table 2: 50%, 90% and 99% drug effective doses**

	ED <sub>50</sub>	ED <sub>90</sub>	ED <sub>99</sub>
	mg/day (95%CI <sup>1</sup> )	mg/day (95%CI <sup>1</sup> )	mg/day (95%CI <sup>1</sup> )
<b>Preemptive therapy</b>			
10 <sup>4</sup> TCID <sub>50</sub>	34 (30-37)	42 (38-46)	53 (48-58)
10 <sup>5</sup> TCID <sub>50</sub>	26 (21-30)	37 (31-44)	56 (46-65)
10 <sup>6</sup> TCID <sub>50</sub>	15 (10-20)	31 (21-41)	70 (48-93)
<b>Preventive therapy</b>			
10 <sup>4</sup> TCID <sub>50</sub>	27 (25-29)	35 (32-38)	47 (44-51)

<sup>1</sup>: 95% confidence interval

Dose-response curves are presented in Figure S2.

133 In a second set of experiments, we assessed, over a period of 7 days, the impact of treatment on the  
134 clinical course of the disease using weight loss as the primary criterion (Figure 3a). Beforehand, we  
135 evaluated the toxicity of the three doses of favipiravir with groups of four non-infected animals treated  
136 from day 0 to day 3 (Figure 3b). High toxicity was observed with the dose of 75mg/day TID with  
137 significant weight loss noticed from the first day of treatment (Table S4). We also found a constant,  
138 but moderate, toxicity with the dose of 37.5mg/day TID that was significant at day 4 and 5 only. No  
139 toxicity was detected with the lower dose of favipiravir. To assess if the toxicity observed with the  
140 highest dose of favipiravir was exacerbated by the infection, we compared weight losses of infected  
141 and non-infected animals treated with the dose of 75mg/day TID. Regardless of the dose of virus, no  
142 significant difference was observed at 1, 2 and 3 dpi (Figure S3). After this evaluation of favipiravir  
143 toxicity, we intranasally infected groups of 10 animals with two doses of virus (10<sup>5</sup> or 10<sup>4</sup> TCID<sub>50</sub>).  
144 Treatment with a dose of 37.5mg/day TID was initiated on the day of infection (preemptive antiviral  
145 therapy) and ended at 3 dpi (Figure 3a). With both doses of virus, treatment was associated with  
146 clinical alleviation of the disease (Figure 3c-d). With the dose of 10<sup>5</sup> TCID<sub>50</sub>, mean weights of treated  
147 animals were significantly higher than those of untreated animals at 5 and 6 dpi ( $p \leq 0.031$ ). Similar  
148 observations were made with the dose of 10<sup>4</sup> TCID<sub>50</sub> at 5, 6 and 7 dpi ( $p < 0.0001$ ).



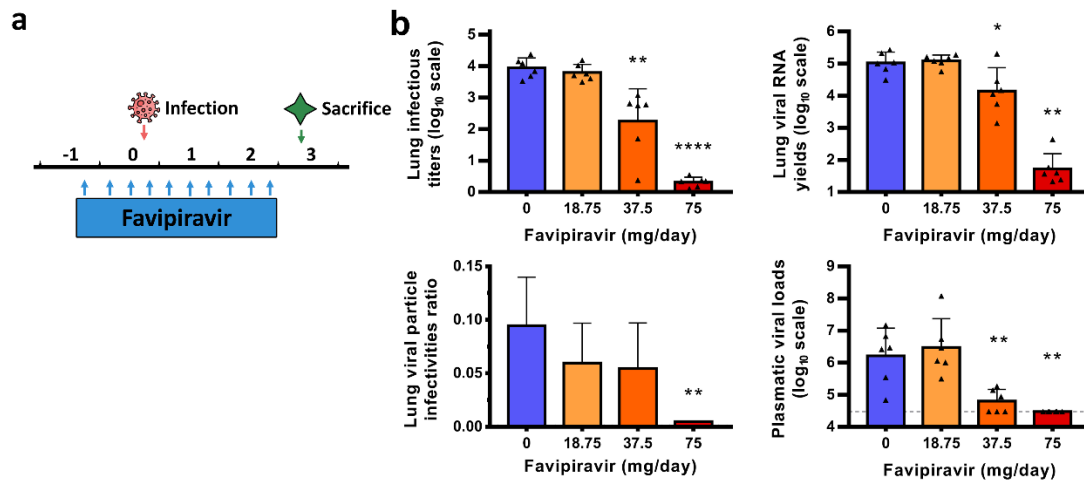
149

150 **Figure 3: Clinical follow-up with preemptive favipiravir therapy**

151 **a** Experimental timeline. **b** Evaluation of the toxicity of the three doses of favipiravir (mg/day TID) with uninfected  
 152 animals following an identical experimental timeline without infection. **c-d** Clinical follow-up with animals  
 153 infected respectively with  $10^5$  and  $10^4$  TCID<sub>50</sub> of virus and treated with a dose of favipiravir of 37.5mg/day TID.  
 154 Normalized weight at day  $n$  was calculated as follows: (% of initial weight of the animal at day  $n$ )/(mean % of  
 155 initial weight for mock-infected animals at day  $n$ ). Data represent mean  $\pm$ SD. \*\*\*\* and \* symbols indicate a  
 156 significant difference between treated and untreated animals with a  $p$ -value  $<0.0001$  and ranging between 0.01-  
 157 0.05 respectively (details in Table S2 and S4).

158 In a third set of experiments, treatment was started one day before infection (preventive antiviral  
 159 therapy) and ended at 2 dpi. We intranasally infected groups of 6 animals with  $10^4$  TCID<sub>50</sub> of virus and  
 160 viral replication was measured in lungs and plasma at 3 dpi (Figure 4a). Once again, an inverse  
 161 relationship was observed between lung infectious titers and the dose of favipiravir (Figure 4b). Mean  
 162 infectious titers for groups of animals treated with 37.5 and 75mg/day TID were significantly lower  
 163 than those observed with untreated groups ( $p \leq 0.002$ ). Of note, undetectable infectious titers were  
 164 found for all animals treated with the higher dose. Estimated ED<sub>90</sub> and ED<sub>99</sub> were 35 and 47mg/day  
 165 respectively (Table 2). Significant reductions of viral RNA yields of 0.9 and 3.3 log<sub>10</sub>, were observed with  
 166 animals treated with 37.5 and 75mg/day TID respectively ( $p \leq 0.023$ ). Resulting infectivity of viral  
 167 particle was decreased, with a significant reduction only for the higher dose of favipiravir ( $p = 0.005$ ).  
 168 Finally, we found significantly reduced plasmatic viral loads with animals treated with 37.5 and  
 169 75mg/day TID ( $p \leq 0.005$ ).





170

#### 171 **Figure 4: Virological results with preventive favipiravir therapy**

172 **a** Experimental timeline. **b** Viral replication in lungs and plasma. Hamsters were intranasally infected with  $10^4$   
173  $TCID_{50}$  of virus. Lung infectious titers (measured using a  $TCID_{50}$  assay) and viral RNA yields were (measured  
174 using an RT-qPCR assay). They are expressed in  $TCID_{50}/copy$  of  $\gamma$ -actine gene and viral genome copies/ $copy$  of  
175  $\gamma$ -actine gene respectively. Relative lung virus infectivities were calculated as follows: ratio of lung infectious titer  
176 over viral RNA yields. Plasmatic viral loads (measured using an RT-qPCR assay) are expressed in viral genome  
177 copies/mL of plasma (the dotted line indicates the detection threshold of the assay). Data represent mean  $\pm$ SD.  
178 \*\*\*\*, \*\* and \* symbols indicate that the average value for the group is significantly different from that of the  
179 untreated group with a p-value  $<0.0001$ , ranging between 0.001-0.01 and 0.01-0.05 respectively (details in Table  
180 S2 and S3).

#### 181 **Favipiravir pharmacokinetics (PK) in a hamster model**

182 We first assessed the PK and lung distribution of favipiravir in a subgroup of uninfected animals. Groups  
183 of animals were treated respectively with a single dose of favipiravir administered intraperitoneally:  
184 6.25mg, 12.5 mg and 25 mg. In each dose group, we sacrificed 3 animals at specific time points post-  
185 treatment (0.5, 1, 5 or 8 hours) for determination of favipiravir in plasma. Drug concentration in lung  
186 tissue was determined at 0.5 and 5 hours post-treatment. Subsequently, we assessed the favipiravir  
187 concentration after multiple dose in animals intranasally infected with  $10^5$   $TCID_{50}$  of virus. Groups of 9  
188 animals received the three doses evaluated for 3 days (Figure 2a): 18.75mg/day, 37.5mg/day and  
189 75mg/day TID and were sacrificed at 12-hours after the last treatment dose. Favipiravir was quantified  
190 in plasma (n=9) and lung tissue (n=3).

191 Results are presented in Table 3 and Figure S4. The single dose PK analysis showed that the maximum  
192 concentration of favipiravir was observed at 0.5 hour at all doses, then plasma drug concentrations  
193 decreased exponentially to reach concentrations below  $10 \mu g/ml$  at 12 hours. Favipiravir PK exhibited  
194 a non-linear increase in concentration between the doses. After multiple doses, trough concentrations  
195 (12 hours) of favipiravir also exhibited a non-linear increase between doses. The extrapolated 12 hours  
196 post-treatment concentrations after a single dose were calculated in order to determine the

197 accumulation ratio. Accumulation ratios were respectively 6, 16 and 21 at the 3 doses, confirming the  
 198 non-proportional increase between doses. The average concentration after single dose administration  
 199 over 0 to 12-hour intervals was calculated and the respective values obtained were 10.1 µg/mL, 38.7  
 200 µg/mL and 100.5 µg/mL for the 3 favipiravir doses.  
 201 Favipiravir lung concentrations were 1.6 to 2.7-fold lower than in plasma for both administration of  
 202 single and multiple doses. After a single dose, the mean lung to plasma ratio ranged from 0.37 to 0.62  
 203 according to the time post-treatment and was similar between the 3 doses of favipiravir at 0.5 hours.  
 204 A high ratio 5 hours post-treatment was observed at the highest dose (25 mg) with an increase by a  
 205 factor 1.6 to 1.8 compared with the lower doses. After multiple doses, the lung penetration of  
 206 favipiravir was confirmed with a mean lung to plasma ratio ranging from 0.35 to 0.44. Favipiravir was  
 207 not detected in the lungs at the lowest dose (18.75 mg/day).

208 **Table 3: Plasma and lung concentrations of favipiravir after administration of a single dose or multiple**  
 209 **dose of favipiravir**

	Single Dose			Multiple Dose <sup>1</sup> (Day 3)		
	Plasma (µg/mL)	Lung (µg/g)	L/p ratio	Plasma (µg/mL)	Lung (µg/g)	L/p ratio
<b>Dose: 25 mg</b>						
0.5 hr	372 ± 47.5	216 ± 39	0.58 ± 0,04			
1 hr	279 ± 49.9					
5 hr	135 ± 49.0	81,3 ± 24	0.62 ± 0,10			
8 hr	5.77 ± 1.34					
12 hr	1.43 <sup>2</sup>			29.9 ± 9.83	16.0 ± 4.87	0.44 ± 0,07
<b>Dose: 12.5 mg</b>						
0.5 hr	166 ± 52.0	90.7 ± 12.7	0.58 ± 0.14			
1 hr	155 ± 20.6					
5 hr	10.7 ± 5.16	3.84 ± 1.49	0.37 ± 0.052			
8 hr	1.94 ± 0.06					
12 hr	0.16 <sup>2</sup>			2.57 ± 1.22	1.36 ± 0.14	0.35 ± 0,03
<b>Dose: 6.25 mg</b>						
0.5 hr	86.3 ± 4.11	50.2 ± 16.4	0.58 ± 0.17			
1 hr	35.2 ± 27.8					
5 hr	2.90 ± 0.25	1.09 ± 0.05	0.38 ± 0.05			
8 hr	0.56 ± 0.16					
12 hr	0.05 <sup>2</sup>			0.31 ± 0.14	not detected	<i>n.a.</i>

210 Data represent mean ±SD; Three animals for each condition except at multiple dose (n=9 for plasma; n=3 for  
 211 lung); details in Table S5

212 <sup>1</sup>: PK realized after 3 days of favipiravir administered three times a day (18.75, 37.5 or 75mg/day TID)

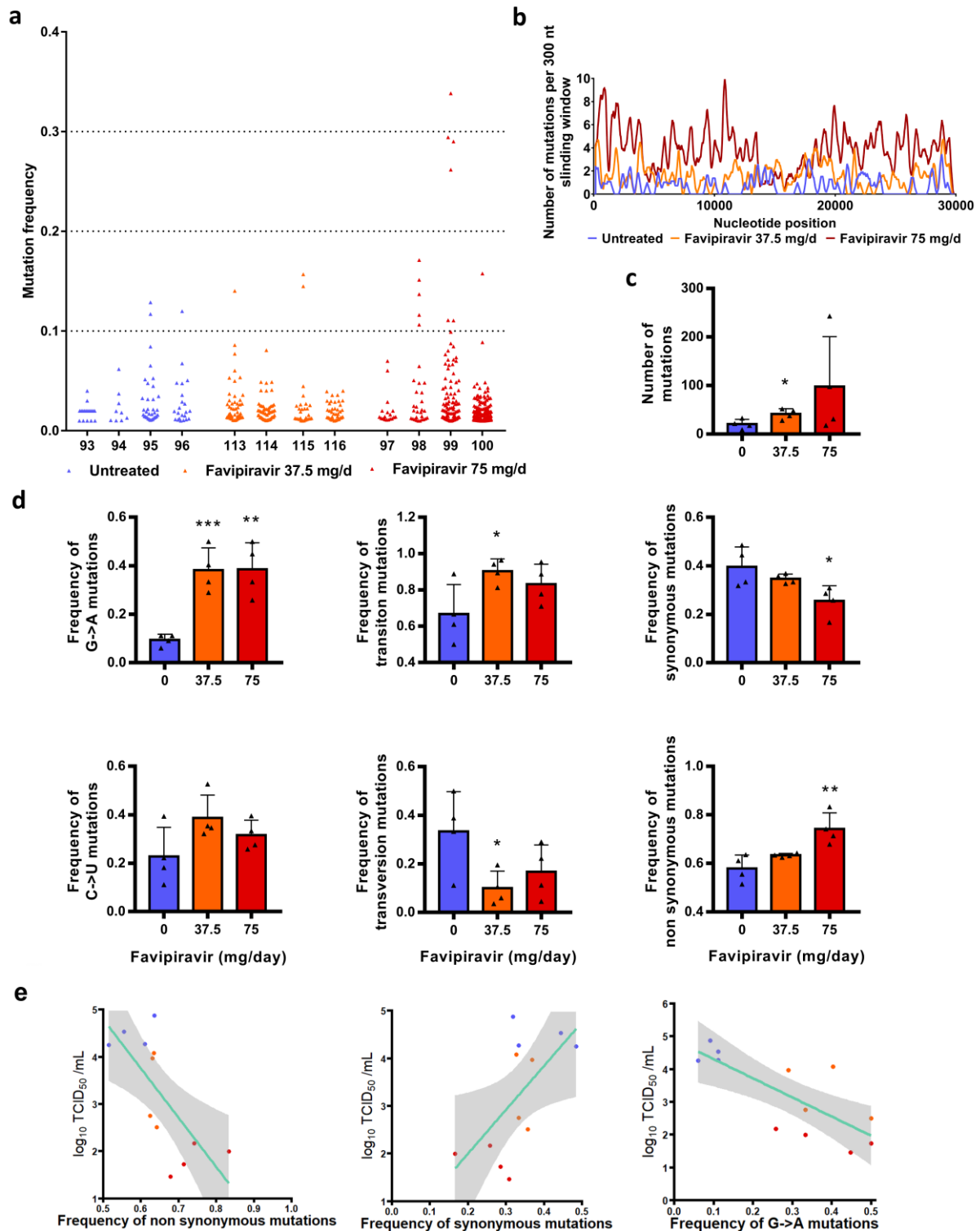
213 <sup>2</sup>: extrapolated C<sub>12h</sub>. *na*: not applicable

## 214 Mutagenic effect of favipiravir

215 To understand which genomic modifications accompanied favipiravir treatment, direct complete  
216 genome sequencing of clarified lung homogenates from animals intranasally infected with  $10^6$  TCID<sub>50</sub>  
217 of virus and treated with the two highest doses of drug (preemptive antiviral therapy; Figure 2) was  
218 performed. Data were generated by next generation sequencing from lung samples of four animals  
219 per group (untreated, 37.5mg/day TID and 75mg/day TID). The mean sequencing coverage for each  
220 sample ranged from 10,991 to 37,991 reads per genomic position and we subjected substitutions with  
221 a frequency  $\geq 1\%$  to further analysis. The genetic variability in virus stock was also analyzed: 14  
222 nucleotide polymorphisms were detected of which 5 recorded a mutation frequency higher than 10%  
223 (Table S6).

224 In order to study the mutagenic effect of favipiravir, we used the consensus sequence from virus stock  
225 as reference and all the mutations simultaneously detected in a lung sample and in virus stock were  
226 not considered in the further analysis (1 to 4 mutations per sample, see Table S6). Overall, no majority  
227 mutations were detected (mutation frequency  $>50\%$ ), mutations were distributed throughout the  
228 whole genome and almost all of them exhibited a frequency lower than 10% (Figure 5a and 5b).

229 Results revealed a relationship between the number of mutations detected per sample and the dose  
230 of favipiravir (Figure 5c): the mean number of mutations increased by a factor 2 and 4.8 with groups  
231 of animals treated with 37.5 and 75mg/day TID, respectively. The difference is significant only with a  
232 dose of 37.5mg/day TID ( $p=0.029$ ). This increase of the number of mutations is mainly the consequence  
233 of the occurrence of a large number of G→A substitutions and, to a lesser extent, C→U substitutions.  
234 Consequently, regardless of the dose of favipiravir, mean frequency of G→A substitutions was  
235 significantly increased by a factor of 4.2 ( $p\leq 0.009$ ). This rise of these transition mutations led to  
236 increased frequency of all transition mutations (significant only at dose of 37.5mg/day TID;  $p=0.037$ )  
237 and increased frequency of non-synonymous mutations (significant only at dose of 75mg/day TID;  
238  $p=0.009$ ) (Figure 5d). We investigated whether or not effectiveness in treated animals was linked with  
239 the characteristics of the mutations detected on viral populations and found that frequency of non-  
240 synonymous, synonymous and G→A mutations were associated with infectious titers in lungs ( $p<0.03$ ;  
241 Figure 5e). Finally, our experiments revealed some parallel evolution events; 32 substitutions in viral  
242 sub-populations were detected in two independent animals. Notably, 18 of these shared mutations  
243 were detected only with treated animals, 14 of them being non-synonymous (Table S8). These  
244 mutations are located in nsp2, 3, 4, 5, 6, 14, N protein, Matrix, ORF 3a and 8. At this stage, one cannot  
245 conclude if these substitutions reflect the adaptation to the hamster model or are the result of the  
246 antiviral selection.



247

248 **Figure 5: Mutagenic effect of favipiravir**

249 **a** Viral genetic diversity in clarified lung homogenates. For each condition, four samples were analyzed. Each  
 250 triangle represents a mutation (only substitutions with a frequency  $\geq 1\%$  were considered). **b** Patterns of mutation  
 251 distribution on complete viral genome. Each variable nucleotide position was counted only once when found.  
 252 The variability was represented using 75 nt sliding windows. For each condition, variable nucleotide positions  
 253 were determined and represented using a 300 nt sliding window. **c** Mean number of mutations. Data represent

254 mean  $\pm$ SD. **d** Mutation characteristics. For each sample, the frequency of a given mutation was calculated as  
255 follows: number of this kind of mutation detected in the sample divided by the total number of mutations  
256 detected in this sample. Data represent mean  $\pm$ SD. \*\* and \* symbols indicate that the average value for the group  
257 is significantly different from that of the untreated group with a p-value ranging between 0.001-0.01 and 0.01-  
258 0.05 respectively (details in details in Table S6 and S7). **e** Association between lung infectious titers (measured  
259 using a TCID<sub>50</sub> assay) and frequency of non synonymous, synonymous and G→A mutations. Each dot represent  
260 data from a given animal.

## 261 Discussion

262 In the current study, we used a hamster model to assess efficacy of the favipiravir against SARS-CoV-  
263 2. Following infection, viral RNA was mainly detected in lungs, blood, and, to a lesser extent, in the  
264 large bowel. Peak of viral replication was observed at 2-3 dpi followed by observation of significant  
265 weight losses, in line with recently reported investigations that involved 6-10 weeks old hamsters  
266 (Kaptein et al., 2020, Chan et al., 2020). Clinically, the main symptom was weight loss, observed from  
267 the first day of infection and followed by recovery at 6dpi. This confirmed that the *in vivo* model, with  
268 younger animals (4 weeks-old), is suitable for preclinical evaluation of antiviral compounds against  
269 SARS-CoV-2.

270 Using a preemptive strategy, we demonstrated that doses of favipiravir of around 700-1400mg/kg/day  
271 TID reduced viral replication in lungs of infected animals and allowed clinical alleviation of the disease.  
272 Reduction of viral replication was greater when estimated on the basis of infectious titers than on total  
273 viral RNA as previously observed in non-human primates treated with Remdesivir (Williamson et al.,  
274 2020). However, the effective doses of favipiravir were higher than those usually used in rodent models  
275 ( $\approx$ 100-400mg/kg/day) (Sidwell et al., 2007, Smither et al., 2014, Julander et al., 2009, Tani et al., 2018,  
276 Oestereich et al., 2016, Yamada et al., 2019). This can be correlated with the high favipiravir EC<sub>50</sub> found  
277 *in vitro* for SARS-CoV-2. Moreover, effective doses were associated with significant toxicity in our  
278 hamster model. This observed toxicity reflected only the adverse effects of favipiravir and was not  
279 exacerbated during SARS-CoV-2 infection. Indeed, similar weight losses were measured among  
280 infected and non-infected animals treated with the highest dose of favipiravir at 1, 2 and 3dpi.

281 In the present study, reduction of viral replication was correlated with the dose of favipiravir  
282 administrated and inversely correlated with the dose of virus inoculated. In a recent study, favipiravir  
283 administrated *per os* twice daily (loading dose of 600mg/kg/day followed by 300mg/kg/day) revealed  
284 a mild reduction of lung viral RNA yields using a similar hamster model with high doses of virus ( $2 \times 10^6$   
285 TCID<sub>50</sub>) (Kaptein et al., 2020). These results are in accordance with ours at the lower dose of favipiravir  
286 (around 340mg/kg/day TID).

287 By characterizing the dose response curve, we estimated that the dose required to reduce by 90%  
288 (ED<sub>90</sub>) the level of infectious titers in lungs is in the range of 570-780mg/kg/day. In the most favourable  
289 situation, where high doses were used as a preemptive therapy, favipiravir led to undetectable viral  
290 replication in lung and plasma. These results showed that the use of high doses of favipiravir could  
291 expand its *in vivo* spectrum against RNA viruses.

292 With influenza viruses, favipiravir acts as a nucleotide analogue. It is metabolized intracellularly to its  
293 active form and incorporated into nascent viral RNA strands. This inhibits RNA strand extension and

294 induces abnormal levels of mutation accumulation into the viral genome (Baranovich et al., 2013,  
295 Sangawa et al., 2013). Recently, it was shown *in vitro* that favipiravir has a similar mechanism of action  
296 with SARS-CoV-2 through a combination of chain termination, reduced RNA synthesis and lethal  
297 mutagenesis (Shannon et al., 2020). Our genomic analysis confirmed the mutagenic effect of favipiravir  
298 *in vivo*. Indeed, we found that favipiravir treatment induced appearance of a large number of G→A  
299 and C→U mutations into viral genomes. This was associated to a decrease of viral infectivity probably  
300 because alteration of the genomic RNA disturb the replication capacity. Similar findings were described  
301 *in vitro* and *in vivo* with other RNA viruses (Baranovich et al., 2013, Guedj et al., 2018, Escribano-  
302 Romero et al., 2017, Arias et al., 2014). Of note, we also observed a strong inverse association between  
303 infectious titers in lungs and the proportion of non-synonymous mutations detected in viral  
304 populations. Because random non-synonymous mutations are more deleterious than synonymous  
305 mutations (Cuevas et al., 2012), this suggests that they were randomly distributed over the three  
306 positions of the codons and that no compensatory mechanism was triggered by the virus to eliminate  
307 them (*i.e.* negative selection). Finally, the inverse correlation between lung infections titers and the  
308 frequency of G→A substitutions showed that an increased proportion of these mutations beyond an  
309 error threshold might be expected to cause lethal mutagenesis.

310 Genomic analyses revealed that 18 mutations detected in viral sub-populations were shared only with  
311 treated animals. Two of them were located in the nsp14 coding region involved in the proof-reading  
312 activity of the viral RNA polymerisation (Eckerle et al., 2007, Ferron et al., 2018). However, they were  
313 located in the N7 MTase domain involved in viral RNA capping (Chen et al., 2013, Ma et al., 2015). By  
314 comparison, resistance mutations selected against Remdesivir in  $\beta$ -coronavirus murine hepatitis virus  
315 model were obtained in the RdRP (nsp12) coding sequence (Agostini et al., 2018). Further  
316 investigations are needed to assess the impact of these mutations on the antiviral effect of favipiravir.  
317 Favipiravir PK in our hamster model displayed a non-linear increase in plasma exposure between the  
318 doses as already reported in nonhuman primates (Madelain et al., 2017). The observed favipiravir  
319 concentration versus time profiles were in agreement with previous results of a PK study performed  
320 in 7-8 week-old hamsters orally treated with a single dose of 100mg/kg of favipiravir (Gowen et al.,  
321 2015). The maximum plasma drug concentration occurred at 0.5 h after oral administration, earlier  
322 than in humans, and then decreased rapidly in agreement with its short half-life (Madelain et al., 2016).  
323 After repeated doses, plasma exposure confirmed non-linear PK over the entire range of doses, further  
324 emphasized by accumulation ratios. The important accumulation observed at the highest dose could  
325 explain in part the toxicity observed in hamsters at this dose. Favipiravir undergoes an important  
326 hepatic metabolism mainly by aldehyde oxidase producing an inactive M1 metabolite and inhibits  
327 aldehyde oxidase activity in a concentration- and time-dependent manner. These properties explain

328 the self-inhibition of its own metabolism as observed in our study in which the highest dose of  
329 favipiravir led to a greater increase in favipiravir concentrations (Madelain et al., 2020).

330 A good penetration of favipiravir in lungs was observed with lung/plasma ratios ranging from 35 to  
331 44% after repeated doses, consistent with its physicochemical properties. Lung exposure was also in  
332 accordance with previous studies (Gowen et al., 2015).

333 How clinically realistic are these results? To address this question we compared the drug  
334 concentrations obtained in the hamster model with those obtained in patients. In 2016, a clinical trial  
335 evaluated the use of favipiravir in Ebola infected patients (Sissoko et al., 2016). The dose used in Ebola  
336 infected patients was 6000mg on day 0 followed by 1200mg BID for 9 days. The median trough  
337 concentrations of favipiravir at Day 2 and Day 4 were 46.1 and 25.9µg/mL, respectively. This is within  
338 the range observed here in hamsters treated with the highest dose (around 1400mg/kg/day), with a  
339 mean trough concentration of 29.9µg/mL. However, additional investigations are required to  
340 determine whether or not similar favipiravir plasma exposure in SARS-COV-2 infected patients are  
341 associated with antiviral activity. The major differences in PK between hamster and humans, and the  
342 toxicity observed at the highest doses in our animal model limits the extrapolation of our results.  
343 Therefore, whether safe dosing regimens in humans may achieve similar plasma exposure and  
344 recapitulate the profound effect on viral replication is unknown. Further, the intracellular  
345 concentration of the active metabolite was not determined and which parameter of the drug  
346 pharmacokinetics best drives the antiviral effect remains to be established.

347 In summary, this study establishes that high doses of favipiravir are associated with antiviral activity  
348 against SARS-CoV-2 infection in a hamster model. The better antiviral efficacy was observed using a  
349 preventive strategy, suggesting that favipiravir could be more appropriate for a prophylactic use. Our  
350 results should be interpreted with caution because high doses of favipiravir were associated with signs  
351 of toxicity in our model. It is required to determine if a tolerable dosing regimen could generate similar  
352 exposure in non-human primates, associated with significant antiviral activity, before testing a high  
353 dose regimen in COVID-19 patients. Furthermore, subsequent studies should determine if an increased  
354 antiviral efficacy can be reached using favipiravir in association with other effective antiviral drugs,  
355 since this strategy may enable to reduce the dosing regimen of favipiravir. Finally, this work reinforces  
356 the need for rapid development of animal models to confirm *in vivo* efficacy of antiviral compounds  
357 and accordingly, to determine appropriate dose regimens in humans before starting clinical trials.



## 358 Acknowledgments

359 We thank Laurence Thirion (UVE; Marseille) for providing RT-qPCR systems . We thank Camille Placidi  
360 (UVE; Marseille) for her technical contribution. We also thank Pr. Ernest A. Gould (UVE; Marseille) for  
361 his careful reading of the manuscript and English language editing. We thank Pr Drosten and Pr Drexler  
362 for providing the SARS-CoV-2 strain through the European Research infrastructure EVA GLOBAL. This  
363 work was supported by the Fondation de France “call FLASH COVID-19”, project TAMAC, by “Institut  
364 national de la santé et de la recherche médicale” through the REACTing (REsearch and ACTion targeting  
365 emerging infectious diseases) initiative (“Preuve de concept pour la production rapide de virus  
366 recombinant SARS-CoV-2”), and by European Virus Archive Global (EVA 213 GLOBAL) funded by the  
367 European Union’s Horizon 2020 research and innovation program under grant agreement No. 871029.  
368 A part of the work was done on the Aix Marseille University antivirals platform “AD2P”.

## 369 Author Contributions

370 Conceptualization, J.S.D., M.C., G.M. and A.N. ; Methodology, J.S.D., M.C., G.L., G.M. and A.N. ; Formal  
371 Analysis, J.S.D., M.C. and G.L. ; Investigation, J.S.D., M.C., G.M., F.T., P.R.P., G.P., K.B. and A.N. ;  
372 Resources, F.T., B.C., J.G., X.d.L., C.S. and A.N. ; Writing – Original Draft, J.S.D., M.C., J.G., C.S. and A.N.  
373 ; Writing – Review & Editing, J.G., X.d.L., C.S. and A.N. ; Visualization, J.S.D., M.C., G.L., F.T., P.R.P. and  
374 A.N. ; Supervision, A.N. ; Funding Acquisition, F.T., B.C., X.d.L. and A.N.

## 375 Declaration of Interests

376 J.G has consulted for F. Hoffman-La Roche. C.S has consulted for ViiV Healthcare, MSD and Gilead.  
377 The remaining authors declare no competing interests.

## 378 Methods

### 379 Cells

380 VeroE6 cells (ATCC CRL-1586) and Caco-2 cells (ATCC HTB-37) were grown at 37°C with 5% CO<sub>2</sub> in  
381 minimal essential medium (MEM) supplemented with 7.5% heat-inactivated fetal bovine serum (FBS),  
382 1% Penicillin/Streptomycin and 1% non-essential amino acids (all from ThermoFisher Scientific).

### 383 Virus

384 All experiments with infectious virus were conducted in biosafety level (BSL) 3 laboratory. SARS-CoV-2  
385 strain BavPat1, supplied through European Virus Archive GLOBAL (<https://www.european-virus->  
386 [archive.com/](https://www.european-virus-archive.com/)), was provided by Christian Drosten (Berlin, Germany). Virus stocks were prepared by  
387 inoculating at MOI of 0.001 a 25cm<sup>2</sup> culture flask of confluent VeroE6 cells with MEM medium  
388 supplemented with 2.5% FBS. The cell supernatant medium was replaced each 24h hours and  
389 harvested at the peak of infection, supplemented with 25mM HEPES (Sigma), aliquoted and stored at  
390 -80°C.

### 391 *In vitro* determination of EC<sub>50</sub>, EC<sub>90</sub>, CC<sub>50</sub> and infectious titer reductions

392 One day prior to infection, 5×10<sup>4</sup> VeroE6 cells were seeded in 96-well culture plates (5×10<sup>4</sup> cells/well  
393 in 100µL of 2.5% FBS medium (assay medium). The next day, seven 2-fold serial dilutions of favipiravir  
394 (Courtesy of Toyama-Chemical; 0.61µg/mL to 78.5µg/mL, in triplicate) were added (25µL/well, in assay  
395 medium). Eight virus control wells were supplemented with 25µL of assay medium and eight cell  
396 controls were supplemented with 50µL of assay medium. After 15 min, 25µL of virus suspension,  
397 diluted in assay medium, was added to the wells at an MOI of 0.01 or 0.001 (except for cell controls).  
398 Three days after infection, cell supernatant media were collected to perform TCID<sub>50</sub> assay (at  
399 concentration of 78.5, 39.3, 19.6µg/mL), as described below, in order to calculate infectious titer  
400 reductions and cell viability was assessed using CellTiter-Blue reagent (Promega) following  
401 manufacturer's instructions. Fluorescence (560/590nm) was recorded with a Tecan Infinite 200Pro  
402 machine (Tecan). The 50% and 90% effective concentrations (EC<sub>50</sub>, EC<sub>90</sub>) were determined using  
403 logarithmic interpolation (% of inhibition were calculated as follows:  $(OD_{\text{sample}} - OD_{\text{virus control}}) / (OD_{\text{cell control}} -$   
404  $OD_{\text{virus control}})$ ). For the evaluation of CC<sub>50</sub> (the concentration that induced 50% cytotoxicity), the same  
405 culture conditions were set as for the determination of the EC<sub>50</sub>, without addition of the virus, then  
406 cell viability was measured using CellTiter Blue (Promega). CC<sub>50</sub> was determined using logarithmic  
407 interpolation.

## 408 *In vivo* experiments

### 409 Approval and authorization

410 *In vivo* experiments were approved by the local ethical committee (C2EA—14) and the French  
411 'Ministère de l'Enseignement Supérieur, de la Recherche et de l'Innovation' (APAFIS#23975) and  
412 performed in accordance with the French national guidelines and the European legislation covering  
413 the use of animals for scientific purposes. All experiments were conducted in BSL 3 laboratory.

### 414 Animal handling

415 Three-week-old female Syrian hamsters were provided by Janvier Labs. Animals were maintained in  
416 ISOcage P - Bioexclusion System (Techniplast) with unlimited access to water/food and 14h/10h  
417 light/dark cycle. Animals were weighed and monitored daily for the duration of the study to detect the  
418 appearance of any clinical signs of illness/suffering. Virus inoculation was performed under general  
419 anesthesia (isoflurane). Organs and blood were collected after euthanasia (cervical dislocation) which  
420 was also realized under general anesthesia (isoflurane).

### 421 Hamster Infection

422 Anesthetized animals (four-week-old) were intranasally infected with 50µL containing 10<sup>6</sup>, 10<sup>5</sup> or  
423 10<sup>4</sup> TCID<sub>50</sub> of virus in 0.9% sodium chloride solution). The mock group was intranasally inoculated with  
424 50µL of 0.9% sodium chloride solution.

### 425 Favipiravir administration

426 Hamster were intra-peritoneally inoculated with different doses of favipiravir. Control group were  
427 intra-peritoneally inoculated with a 0.9% sodium chloride solution.

### 428 Organ collection

429 Organs were first washed in 10mL of 0.9% sodium chloride solution and then transferred to a 2mL or  
430 50mL tube containing respectively 1mL (small/large bowel pieces, kidney, spleen and heart) or 10mL  
431 (lungs, brain and liver) of 0.9% sodium chloride solution and 3mm glass beads. They were crushed  
432 using a the Tissue Lyser machine (Retsch MM400) for 5min at 30 cycles/s and then centrifuged 5min à  
433 1200g. Supernatant media were transferred to a 2mL tube, centrifuged 10 min at 16,200g and stored  
434 at -80°C. One milliliter of blood was harvested in a 2mL tube containing 100µL of 0.5M EDTA  
435 (ThermoFischer Scientific). Blood was centrifuged for 10 min at 16,200g and stored at -80°C.

### 436 **Quantitative real-time RT-PCR (RT-qPCR) assays**

437 To avoid contamination, all experiments were conducted in a molecular biology laboratory that is  
438 specifically designed for clinical diagnosis using molecular techniques, and which includes separate  
439 laboratories dedicated to perform each step of the procedure. Prior to PCR amplification, RNA  
440 extraction was performed using the QIAamp 96 DNA kit and the Qiacube HT kit and the Qiacube HT

441 (both from Qiagen) following the manufacturer's instructions. Shortly, 100  $\mu$ l of organ clarified  
442 homogenates, spiked with 10  $\mu$ l of internal control (bacteriophage MS2) (Ninove et al., 2011), were  
443 transferred into an S-block containing the recommended volumes of VXL, proteinase K and RNA carrier.  
444 RT-qPCR (SARS-CoV-2 and MS2 viral genome detection) were performed with the Express one step RT-  
445 qPCR Universal kit (ThermoFisher Scientific) using 3.5  $\mu$ l of RNA and 6.5  $\mu$ l of RT-qPCR mix that contains  
446 250nmol of each primer and 75nmol of probe. Amplification was performed with the QuantStudio 12K  
447 Flex Real-Time PCR System (ThermoFisher Scientific) using the following conditions: 50°C for 10min,  
448 95°C for 20s, followed by 40 cycles of 95°C for 3s, 60°C for 30s. qPCR ( $\gamma$ -actine gene detection) was  
449 performed under the same condition as RT-qPCR with the following modifications: we used the Express  
450 one step qPCR Universal kit (ThermoFisher Scientific) and the 50°C step of the amplification cycle was  
451 removed. Primers and probes sequences used to detect SARS-CoV-2, MS2 and  $\gamma$ -actine are described  
452 in Table S9.

#### 453 Tissue-culture infectious dose 50 (TCID<sub>50</sub>) assay

454 To determine infectious titers, 96-well culture plates containing confluent VeroE6 cells were  
455 inoculated with 150  $\mu$ l per well of serial dilutions of each sample (four-fold or ten-fold dilutions when  
456 analyzing lung clarified homogenates or cell supernatant media respectively). Each dilution was  
457 performed in sextuplicate. Plates were incubated for 4 days and then read for the absence or presence  
458 of cytopathic effect in each well. Infectious titers were estimated using the method described by Reed  
459 & Muench (REED and MUENCH, 1938).

#### 460 Favipiravir pharmacokinetics

461 Animal handling, hamster infections and favipiravir administrations were performed as described  
462 above. A piece of left lung was first washed in 10mL of sodium chloride 0.9% solution, blotted with  
463 filter paper, weighed and then transferred to a 2mL tube containing 1mL of 0.9% sodium chloride  
464 solution and 3mm glass beads. It was crushed using the Tissue Lyser machine (Retsch MM400) during  
465 10min at 30 cycles/s and then centrifuged 5min à 1200g. Supernatant media were transferred to 2mL  
466 tubes, centrifuged 10 min at 16,200g and stored at -80°C. One milliliter of blood was harvested in a  
467 2mL tube containing 100  $\mu$ l of 0.5M EDTA (ThermoFischer Scientific). Blood was centrifuged for 10 min  
468 at 16,200g and stored at -80°C.

469 Quantification of favipiravir in plasma and lung tissues was performed by a validated sensitive and  
470 selective validated high-performance liquid chromatography coupled with tandem mass spectrometry  
471 method (UPLC-TQD, Waters, USA) with a lower limit of quantification of 0.1  $\mu$ g/mL. Precision and  
472 accuracy of the 3 quality control samples (QCs) were within 15% over the calibration range (0.5  $\mu$ g/mL  
473 to 100  $\mu$ g/mL) (Bekegnran *et al.*, submitted). Favipiravir was extracted by a simple protein precipitation  
474 method, using acetonitrile for plasma and ice-cold acetonitrile for clarified lung homogenates. Briefly,

475 50  $\mu$ L of samples matrix was added to 500 $\mu$ L of acetonitrile solution containing the internal standard  
476 (favipiravir- $^{13}\text{C},^{15}\text{N}$ , Alsachim), then vortexed for 2min followed by centrifugation for 10min at 4°C.  
477 The supernatant medium was evaporated and the dry residues were then transferred to 96-well plates  
478 and 50  $\mu$ L was injected. To assess the selectivity and specificity of the method and matrix effect, blank  
479 plasma and tissues homogenates from 2 control animals (uninfected and untreated) were processed  
480 at each run. Moreover, the same control samples spiked with favipiravir concentration equivalent to  
481 the QCs (0.75, 50 and 80  $\mu\text{g}/\text{mL}$ ) were also processed and compared to the QCs samples.  
482 Noncompartmental analysis conducted using software Pkanalix2019R2 ([www.lixoft.com](http://www.lixoft.com)). Areas  
483 under the plasma concentration time curve were computed using medians of favipiravir  
484 concentrations at 0.5, 1, 5 and 8 hours, and extrapolated until T=12h.  $C_{\text{trough}}$  were extrapolated at  
485 T=12h using lambda-z loglinear regression on the decreasing slope of concentrations.

#### 486 Sequence analysis of the full-length genome

487 200 $\mu$ L of lung clarified homogenate or infectious cell supernatant (virus stock) was inactivated with an  
488 equal volume of VXL lysis buffer (Qiagen) and viral RNA was extracted using an EZ1 Advanced XL robot  
489 with the EZ1 mini virus 2.0 kit (both from Qiagen) and linear acrylamide (ThermoFisher Scientific) in  
490 place of carrier RNA. cDNA was generated in a final volume of 40 $\mu$ L using 14 $\mu$ L of nucleic acid extract,  
491 random hexamer and the Protoscript II First Strand cDNA Synthesis Kit (New England Biolabs). A  
492 specific set of primers (Table S10) was used to generate thirteen amplicons covering the entire genome  
493 with the Q5 High-Fidelity DNA polymerase (New England Biolabs). PCR mixes (final volume 25 $\mu$ L)  
494 contained 2.5 $\mu$ L of cDNA, 2 $\mu$ L of each primer (10 $\mu\text{M}$ ) and 12.5  $\mu$ L of Q5 High-Fidelity 2X Master Mix.  
495 Amplification was performed with the following conditions: 30 sec at 98°C, then 45 cycles of 15 sec at  
496 98°C and 5 min à 65°C. Size of PCR products was verified by gel electrophoresis. For each sample, an  
497 equimolar pool of all amplicons was prepared and purified using Monarch PCR & DNA Cleanup Kit (New  
498 England Biolabs). After DNA quantification using Qubit dsDNA HS Assay Kit and Qubit 2.0 fluorometer  
499 (ThermoFisher Scientific), amplicons were fragmented by sonication into fragments of around 200bp  
500 long. Libraries were built by adding barcodes, for sample identification, and primers using AB Library  
501 Builder System (ThermoFisher Scientific). To pool equimolarly the barcoded samples a quantification  
502 step by real time PCR using Ion Library TaqMan Quantitation Kit (ThermoFisher Scientific) was  
503 performed. Then, emulsion PCR from pools and loading on 530 chip was performed using the  
504 automated Ion Chef instrument (ThermoFisher Scientific). Sequencing was performed using the S5 Ion  
505 torrent technology v5.12 (ThermoFisher Scientific) following manufacturer's instructions. Consensus  
506 sequence was obtained after trimming of reads (reads with quality score <0.99, and length <100pb  
507 were removed and the 30 first and 30 last nucleotides were removed from the reads). Mapping of the  
508 reads on a reference (determine following blast of De Novo contigs) was done using CLC genomics

509 workbench software v.20 (Qiagen). A *de novo* contig was also produced to ensure that the consensus  
510 sequence was not affected by the reference sequence. Mutation frequency for each position was  
511 calculated as the number of reads with a mutation compared to the reference divided by the total  
512 number of reads at that site. Only substitutions with a frequency of at least 1% were taken into account  
513 for the analysis (Table S6).

#### 514 **ED<sub>50</sub>, ED<sub>90</sub> and ED<sub>99</sub> determination**

515 We conducted a nonlinear regression of infectious viral load against dose, using an E<sub>max</sub> model, giving

516  $VL = VL_0 \times \left( 1 - \left( \frac{D^\gamma}{D^\gamma + D_{50}^\gamma} \right) \right)$  with  $VL_0$  being infectious viral load of untreated animals. We estimated

517  $D_{50}$  the dose required to decrease viral load by 50%, using a coefficient  $\gamma$  to account for the high  
518 sigmoidicity of the relation between dose and titers.  $\gamma$  coefficient was chosen as the one maximizing

519 likelihood of the model. We extrapolated the  $D_{90}$  and  $D_{99}$  using  $D_{90} = \sqrt[\gamma]{9 \times D_{50}^\gamma}$  and  $D_{99} =$

520  $\sqrt[\gamma]{99 \times D_{50}^\gamma}$ , as well as their 95% confidence interval using the delta method.

#### 521 **Statistical analysis**

522 Graphical representations and statistical analyses were performed with Graphpad Prism 7 (Graphpad  
523 software) except linear/nonlinear regressions and their corresponding graphical representations that  
524 were performed using R statistical software (<http://www.R-project.org>). Statistical details for each  
525 experiments are described in the figure legends and in corresponding supplemental tables. P-values  
526 lower than 0.05 were considered statistically significant.

## 527 Supplemental Data

528 Supplemental figure 1: In vitro efficacy of favipiravir

529 Supplemental figure 2: Dose-response curves

530 Supplemental figure 3: Evaluation of the toxicity for animals infected and treated with high doses of  
531 favipiravir

532 Supplemental figure 4: Plasma concentrations of favipiravir after administration of a single dose of  
533 favipiravir

534 Supplemental table 1: Implementation of hamster model

535 Supplemental table 2: Individual data from in vivo experiments

536 Supplemental table 3: Statistical analysis of in vivo experiments

537 Supplemental table 4: Statistical analysis of clinical monitoring

538 Supplemental table 5: Individual data of favipiravir pharmacokinetics

539 Supplemental table 6: Individual data for analysis of mutagenic effect of favipiravir

540 Supplemental table 7: Statistical analysis of mutagenic effect of favipiravir

541 Supplemental table 8: Shared mutations detected in lung clarified homogenates

542 Supplemental table 9: (RT)-qPCR systems

543 Supplemental table 10: Primer sequences used to produce overlapping amplicons for next generation  
544 sequencing

## 545 References

- 546 AGOSTINI, M. L., ANDRES, E. L., SIMS, A. C., GRAHAM, R. L., SHEAHAN, T. P., LU, X., SMITH, E. C., CASE,  
547 J. B., FENG, J. Y., JORDAN, R., RAY, A. S., CIHLAR, T., SIEGEL, D., MACKMAN, R. L., CLARKE, M.  
548 O., BARIC, R. S. & DENISON, M. R. 2018. Coronavirus Susceptibility to the Antiviral Remdesivir  
549 (GS-5734) Is Mediated by the Viral Polymerase and the Proofreading Exoribonuclease. *mBio*,  
550 9.
- 551 ARIAS, A., THORNE, L. & GOODFELLOW, I. 2014. Favipiravir elicits antiviral mutagenesis during virus  
552 replication in vivo. *Elife*, 3, e03679.
- 553 BARANOVICH, T., WONG, S. S., ARMSTRONG, J., MARJUKI, H., WEBBY, R. J., WEBSTER, R. G. &  
554 GOVORKOVA, E. A. 2013. T-705 (favipiravir) induces lethal mutagenesis in influenza A H1N1  
555 viruses in vitro. *J Virol*, 87, 3741-51.
- 556 CHAN, J. F., ZHANG, A. J., YUAN, S., POON, V. K., CHAN, C. C., LEE, A. C., CHAN, W. M., FAN, Z., TSOI, H.  
557 W., WEN, L., LIANG, R., CAO, J., CHEN, Y., TANG, K., LUO, C., CAI, J. P., KOK, K. H., CHU, H.,  
558 CHAN, K. H., SRIDHAR, S., CHEN, Z., CHEN, H., TO, K. K. & YUEN, K. Y. 2020. Simulation of the  
559 clinical and pathological manifestations of Coronavirus Disease 2019 (COVID-19) in golden  
560 Syrian hamster model: implications for disease pathogenesis and transmissibility. *Clin Infect*  
561 *Dis*.
- 562 CHEN, Y., TAO, J., SUN, Y., WU, A., SU, C., GAO, G., CAI, H., QIU, S., WU, Y., AHOLA, T. & GUO, D. 2013.  
563 Structure-function analysis of severe acute respiratory syndrome coronavirus RNA cap  
564 guanine-N7-methyltransferase. *J Virol*, 87, 6296-305.
- 565 CUEVAS, J. M., DOMINGO-CALAP, P. & SANJUAN, R. 2012. The fitness effects of synonymous mutations  
566 in DNA and RNA viruses. *Mol Biol Evol*, 29, 17-20.
- 567 DONG, E., DU, H. & GARDNER, L. 2020. An interactive web-based dashboard to track COVID-19 in real  
568 time. *Lancet Infect Dis*, 20, 533-534.
- 569 ECKERLE, L. D., LU, X., SPERRY, S. M., CHOI, L. & DENISON, M. R. 2007. High fidelity of murine hepatitis  
570 virus replication is decreased in nsp14 exoribonuclease mutants. *J Virol*, 81, 12135-44.
- 571 ESCRIBANO-ROMERO, E., JIMENEZ DE OYA, N., DOMINGO, E. & SAIZ, J. C. 2017. Extinction of West Nile  
572 Virus by Favipiravir through Lethal Mutagenesis. *Antimicrob Agents Chemother*, 61.
- 573 FERRON, F., SUBISSI, L., SILVEIRA DE MORAIS, A. T., LE, N. T. T., SEVAJOL, M., GLUAIS, L., DECROLY, E.,  
574 VONRHEIN, C., BRICOGNE, G., CANARD, B. & IMBERT, I. 2018. Structural and molecular basis  
575 of mismatch correction and ribavirin excision from coronavirus RNA. *Proc Natl Acad Sci U S A*,  
576 115, E162-E171.



- 577 GOWEN, B. B., SEFING, E. J., WESTOVER, J. B., SMEE, D. F., HAGLOCH, J., FURUTA, Y. & HALL, J. O. 2015.  
578 Alterations in favipiravir (T-705) pharmacokinetics and biodistribution in a hamster model of  
579 viral hemorrhagic fever. *Antiviral Res*, 121, 132-7.
- 580 GUEDJ, J., PIORKOWSKI, G., JACQUOT, F., MADELAIN, V., NGUYEN, T. H. T., RODALLEC, A., GUNTHER,  
581 S., CARBONNELLE, C., MENTRE, F., RAOUL, H. & DE LAMBALLERIE, X. 2018. Antiviral efficacy of  
582 favipiravir against Ebola virus: A translational study in cynomolgus macaques. *PLoS Med*, 15,  
583 e1002535.
- 584 HE, X., LAU, E. H. Y., WU, P., DENG, X., WANG, J., HAO, X., LAU, Y. C., WONG, J. Y., GUAN, Y., TAN, X.,  
585 MO, X., CHEN, Y., LIAO, B., CHEN, W., HU, F., ZHANG, Q., ZHONG, M., WU, Y., ZHAO, L., ZHANG,  
586 F., COWLING, B. J., LI, F. & LEUNG, G. M. 2020. Temporal dynamics in viral shedding and  
587 transmissibility of COVID-19. *Nat Med*, 26, 672-675.
- 588 HUANG, C., WANG, Y., LI, X., REN, L., ZHAO, J., HU, Y., ZHANG, L., FAN, G., XU, J., GU, X., CHENG, Z., YU,  
589 T., XIA, J., WEI, Y., WU, W., XIE, X., YIN, W., LI, H., LIU, M., XIAO, Y., GAO, H., GUO, L., XIE, J.,  
590 WANG, G., JIANG, R., GAO, Z., JIN, Q., WANG, J. & CAO, B. 2020. Clinical features of patients  
591 infected with 2019 novel coronavirus in Wuhan, China. *Lancet*, 395, 497-506.
- 592 JEON, S., KO, M., LEE, J., CHOI, I., BYUN, S. Y., PARK, S., SHUM, D. & KIM, S. 2020. Identification of  
593 antiviral drug candidates against SARS-CoV-2 from FDA-approved drugs. *Antimicrob Agents*  
594 *Chemother*.
- 595 JOCHMANS, D., VAN NIEUWKOOP, S., SMITS, S. L., NEYTS, J., FOUCHIER, R. A. & VAN DEN HOOGEN, B.  
596 G. 2016. Antiviral Activity of Favipiravir (T-705) against a Broad Range of Paramyxoviruses In  
597 Vitro and against Human Metapneumovirus in Hamsters. *Antimicrob Agents Chemother*, 60,  
598 4620-9.
- 599 JULANDER, J. G., SHAFER, K., SMEE, D. F., MORREY, J. D. & FURUTA, Y. 2009. Activity of T-705 in a  
600 hamster model of yellow fever virus infection in comparison with that of a chemically related  
601 compound, T-1106. *Antimicrob Agents Chemother*, 53, 202-9.
- 602 KAPTEIN, S. J., JACOBS, S., LANGENDRIES, L., SELDESLACHTS, L., TER HORST, S., LIESENBORGH, L.,  
603 HENS, B., VERGOTE, V., HEYLEN, E., MAAS, E., DE KEYZER, C., BERVOETS, L., RYMENANTS, J.,  
604 VAN BUYTEN, T., THIBAUT, H. J., DALLMEIER, K., BOUDEWIJNS, R., WOUTERS, J., AUGUSTIJNS,  
605 P., VEROUGSTRAETE, N., CAWTHORNE, C., WEYNAND, B., ANNAERT, P., SPRIET, I., VELDE, G.  
606 V., NEYTS, J., ROCHA-PEREIRA, J. & DELANG, L. 2020. Antiviral treatment of SARS-CoV-2-  
607 infected hamsters reveals a weak effect of favipiravir and a complete lack of effect for  
608 hydroxychloroquine. *bioRxiv*, 2020.06.19.159053.
- 609 MA, Y., WU, L., SHAW, N., GAO, Y., WANG, J., SUN, Y., LOU, Z., YAN, L., ZHANG, R. & RAO, Z. 2015.  
610 Structural basis and functional analysis of the SARS coronavirus nsp14-nsp10 complex. *Proc*  
611 *Natl Acad Sci U S A*, 112, 9436-41.

- 612 MADELAIN, V., GUEDJ, J., MENTRE, F., NGUYEN, T. H., JACQUOT, F., OESTEREICH, L., KADOTA, T.,  
613 YAMADA, K., TABURET, A. M., DE LAMBALLERIE, X. & RAOUL, H. 2017. Favipiravir  
614 Pharmacokinetics in Nonhuman Primates and Insights for Future Efficacy Studies of  
615 Hemorrhagic Fever Viruses. *Antimicrob Agents Chemother*, 61.
- 616 MADELAIN, V., MENTRE, F., BAIZE, S., ANGLARET, X., LAOUENAN, C., OESTEREICH, L., NGUYEN, T. H. T.,  
617 MALVY, D., PIORKOWSKI, G., GRAW, F., GUNTHER, S., RAOUL, H., DE LAMBALLERIE, X. &  
618 GUEDJ, J. 2020. Modeling Favipiravir Antiviral Efficacy Against Emerging Viruses: From Animal  
619 Studies to Clinical Trials. *CPT Pharmacometrics Syst Pharmacol*, 9, 258-271.
- 620 MADELAIN, V., NGUYEN, T. H., OLIVO, A., DE LAMBALLERIE, X., GUEDJ, J., TABURET, A. M. & MENTRE,  
621 F. 2016. Ebola Virus Infection: Review of the Pharmacokinetic and Pharmacodynamic  
622 Properties of Drugs Considered for Testing in Human Efficacy Trials. *Clin Pharmacokinet*, 55,  
623 907-23.
- 624 MERCORELLI, B., PALU, G. & LOREGIAN, A. 2018. Drug Repurposing for Viral Infectious Diseases: How  
625 Far Are We? *Trends Microbiol*, 26, 865-876.
- 626 NINOVE, L., NOUGAIREDE, A., GAZIN, C., THIRION, L., DELOGU, I., ZANDOTTI, C., CHARREL, R. N. & DE  
627 LAMBALLERIE, X. 2011. RNA and DNA bacteriophages as molecular diagnosis controls in clinical  
628 virology: a comprehensive study of more than 45,000 routine PCR tests. *PLoS One*, 6, e16142.
- 629 OESTEREICH, L., RIEGER, T., LUDTKE, A., RUIBAL, P., WURR, S., PALLASCH, E., BOCKHOLT, S.,  
630 KRASEMANN, S., MUNOZ-FONTELA, C. & GUNTHER, S. 2016. Efficacy of Favipiravir Alone and  
631 in Combination With Ribavirin in a Lethal, Immunocompetent Mouse Model of Lassa Fever. *J*  
632 *Infect Dis*, 213, 934-8.
- 633 REED, L. J. & MUENCH, H. 1938. A SIMPLE METHOD OF ESTIMATING FIFTY PER CENT ENDPOINTS.  
634 *American Journal of Epidemiology*, 27, 493-497.
- 635 ROCKX, B., KUIKEN, T., HERFST, S., BESTEBROER, T., LAMERS, M. M., OUDE MUNNINK, B. B., DE  
636 MEULDER, D., VAN AMERONGEN, G., VAN DEN BRAND, J., OKBA, N. M. A., SCHIPPER, D., VAN  
637 RUN, P., LEIJTEN, L., SIKKEMA, R., VERSCHOOR, E., VERSTREPEN, B., BOGERS, W.,  
638 LANGERMANS, J., DROSTEN, C., FENTENER VAN VLISSINGEN, M., FOUCHIER, R., DE SWART, R.,  
639 KOOPMANS, M. & HAAGMANS, B. L. 2020. Comparative pathogenesis of COVID-19, MERS, and  
640 SARS in a nonhuman primate model. *Science*, 368, 1012-1015.
- 641 ROSENKE, K., FELDMANN, H., WESTOVER, J. B., HANLEY, P. W., MARTELLARO, C., FELDMANN, F.,  
642 SATURDAY, G., LOVAGLIO, J., SCOTT, D. P., FURUTA, Y., KOMENO, T., GOWEN, B. B. &  
643 SAFRONETZ, D. 2018. Use of Favipiravir to Treat Lassa Virus Infection in Macaques. *Emerg*  
644 *Infect Dis*, 24, 1696-1699.

- 645 SANGAWA, H., KOMENO, T., NISHIKAWA, H., YOSHIDA, A., TAKAHASHI, K., NOMURA, N. & FURUTA, Y.  
646 2013. Mechanism of action of T-705 ribosyl triphosphate against influenza virus RNA  
647 polymerase. *Antimicrob Agents Chemother*, 57, 5202-8.
- 648 SEGURA GUERRERO, N. A., SHARMA, S., NEYTS, J. & KAPTEIN, S. J. F. 2018. Favipiravir inhibits in vitro  
649 Usutu virus replication and delays disease progression in an infection model in mice. *Antiviral*  
650 *Res*, 160, 137-142.
- 651 SHANNON, A., SELISKO, B., LE, N., HUCHTING, J., TOURET, F., PIORKOWSKI, G., FATTORINI, V., FERRON,  
652 F., DECROLY, E., MEIER, C., COUTARD, B., PEERSEN, O. & CANARD, B. 2020. Favipiravir strikes  
653 the SARS-CoV-2 at its Achilles heel, the RNA polymerase. *bioRxiv*, 2020.05.15.098731.
- 654 SIDWELL, R. W., BARNARD, D. L., DAY, C. W., SMEE, D. F., BAILEY, K. W., WONG, M. H., MORREY, J. D.  
655 & FURUTA, Y. 2007. Efficacy of orally administered T-705 on lethal avian influenza A (H5N1)  
656 virus infections in mice. *Antimicrob Agents Chemother*, 51, 845-51.
- 657 SISSOKO, D., LAOUEANAN, C., FOLKESSON, E., M'LEBING, A. B., BEAVOGUI, A. H., BAIZE, S., CAMARA, A.  
658 M., MAES, P., SHEPHERD, S., DANIEL, C., CARAZO, S., CONDE, M. N., GALA, J. L., COLIN, G.,  
659 SAVINI, H., BORE, J. A., LE MARCIS, F., KOUNDOUNO, F. R., PETITJEAN, F., LAMAH, M. C.,  
660 DIEDERICH, S., TOUNKARA, A., POELART, G., BERBAIN, E., DINDART, J. M., DURAFFOUR, S.,  
661 LEFEVRE, A., LENO, T., PEYROUSET, O., IRENGE, L., BANGOURA, N., PALICH, R., HINZMANN, J.,  
662 KRAUS, A., BARRY, T. S., BERETTE, S., BONGONO, A., CAMARA, M. S., MUNOZ, V. C.,  
663 DOUMBOUYA, L., HAROUNA, S., KIGHOMA, P. M., KOUNDOUNO, F. R., LOLAMOU, R., LOUA,  
664 C. M., MASSALA, V., MOUMOUNI, K., PROVOST, C., SAMAKE, N., SEKOU, C., SOUMAH, A.,  
665 ARNOULD, I., KOMANO, M. S., GUSTIN, L., BERUTTO, C., CAMARA, D., CAMARA, F. S.,  
666 COLPAERT, J., DELAMOU, L., JANSSON, L., KOUROUMA, E., LOUA, M., MALME, K., MANFRIN,  
667 E., MAOMOU, A., MILINOULO, A., OMBELET, S., SIDIBOUN, A. Y., VERRECKT, I., YOMBOUNO,  
668 P., BOCQUIN, A., CARBONNELLE, C., CARMOI, T., FRANGE, P., MELY, S., NGUYEN, V. K.,  
669 PANNETIER, D., TABURET, A. M., TRELUYER, J. M., KOLIE, J., MOH, R., GONZALEZ, M. C.,  
670 KUISMA, E., LIEDIGK, B., NGABO, D., RUDOLF, M., THOM, R., KERBER, R., GABRIEL, M., WLFEL,  
671 R., WOLFEL, R., BADIR, J., BENTAHIR, M., DECCACHE, Y., DUMONT, C., DURANT, J. F., EL  
672 BAKKOURI, K., UWAMAHORO, M. G., SMITS, B., TOUFIK, N., et al. 2016. Experimental  
673 Treatment with Favipiravir for Ebola Virus Disease (the JIKI Trial): A Historically Controlled,  
674 Single-Arm Proof-of-Concept Trial in Guinea. *Plos Medicine*, 13.
- 675 SMITHER, S. J., EASTAUGH, L. S., STEWARD, J. A., NELSON, M., LENK, R. P. & LEVER, M. S. 2014. Post-  
676 exposure efficacy of oral T-705 (Favipiravir) against inhalational Ebola virus infection in a  
677 mouse model. *Antiviral Res*, 104, 153-5.

678 TAKAHASHI, K., FURUTA, Y., FUKUDA, Y., KUNO, M., KAMIYAMA, T., KOZAKI, K., NOMURA, N., EGAWA,  
679 H., MINAMI, S. & SHIRAKI, K. 2003. In vitro and in vivo activities of T-705 and oseltamivir against  
680 influenza virus. *Antivir Chem Chemother*, 14, 235-41.

681 TANI, H., KOMENO, T., FUKUMA, A., FUKUSHI, S., TANIGUCHI, S., SHIMOJIMA, M., UDA, A., MORIKAWA,  
682 S., NAKAJIMA, N., FURUTA, Y. & SAIJO, M. 2018. Therapeutic effects of favipiravir against  
683 severe fever with thrombocytopenia syndrome virus infection in a lethal mouse model: Dose-  
684 efficacy studies upon oral administration. *PLoS One*, 13, e0206416.

685 WANG, M., CAO, R., ZHANG, L., YANG, X., LIU, J., XU, M., SHI, Z., HU, Z., ZHONG, W. & XIAO, G. 2020.  
686 Remdesivir and chloroquine effectively inhibit the recently emerged novel coronavirus (2019-  
687 nCoV) in vitro. *Cell Res*, 30, 269-271.

688 WHO 2020. World Health Organization. WHO Director-General's opening remarks at the media  
689 briefing on COVID-19 - 11 March 2020 (<https://www.who.int>).

690 WILLIAMSON, B. N., FELDMANN, F., SCHWARZ, B., MEADE-WHITE, K., PORTER, D. P., SCHULZ, J., VAN  
691 DOREMALEN, N., LEIGHTON, I., YINDA, C. K., PEREZ-PEREZ, L., OKUMURA, A., LOVAGLIO, J.,  
692 HANLEY, P. W., SATURDAY, G., BOSIO, C. M., ANZICK, S., BARBIAN, K., CIHLAR, T., MARTENS,  
693 C., SCOTT, D. P., MUNSTER, V. J. & DE WIT, E. 2020. Clinical benefit of remdesivir in rhesus  
694 macaques infected with SARS-CoV-2. *Nature*.

695 YAMADA, K., NOGUCHI, K., KIMITSUKI, K., KAIMORI, R., SAITO, N., KOMENO, T., NAKAJIMA, N.,  
696 FURUTA, Y. & NISHIZONO, A. 2019. Reevaluation of the efficacy of favipiravir against rabies  
697 virus using in vivo imaging analysis. *Antiviral Res*, 172, 104641.

698 ZHU, N., ZHANG, D., WANG, W., LI, X., YANG, B., SONG, J., ZHAO, X., HUANG, B., SHI, W., LU, R., NIU,  
699 P., ZHAN, F., MA, X., WANG, D., XU, W., WU, G., GAO, G. F., TAN, W., CHINA NOVEL  
700 CORONAVIRUS, I. & RESEARCH, T. 2020. A Novel Coronavirus from Patients with Pneumonia in  
701 China, 2019. *N Engl J Med*, 382, 727-733.

702